ELECTROSTATIC SHIELD TO MITIGATE THE HIGH FREQUENCY CIRCULATING BEARING CURRENT – A STUDY FOR DESIGN GUIDELINES

Marco T. A. Êvo
Electrical Engineering Department
Federal University of São João del Rei
São João del Rei, MG, 36307-352
Brazil
mtevo@ufsj.edu.br

Caio Eduardo Silva
Graduate Program in Electrical Engineering
Federal University of Uberlândia
Uberlândia, MG, Brazil
caioeduardo@ufsj.edu.br

Isabela O. Zaparoli
Graduate Program in Electrical Engineering
Federal University of Uberlândia
Uberlândia, MG, Brazil
oliveirazaparoli@gmail.com

Hélder de Paula
Member, IEEE
Faculty of Electrical Engineering
Federal University of Uberlândia
Uberlândia, MG, Brazil
drhelderdepaula@gmail.com

Abstract – In a previous work, the authors addressed electrostatic shielding to reduce the bearing discharge currents (Electrostatic discharge machining currents - EDM). In order to expand the application of such a shielding device, this paper presents an analysis of its use to reduce the inverter-induced circulating bearing currents on induction machines. Employing finite element analysis (FEA), 2D and 3D models were developed to clarify the tradeoff between the shield effectiveness and the associated additional heat losses and motor efficiency reduction, considering different geometric arrangements and materials for the shielding device construction. The results provide very good guidelines for the shield design, contributing to its practical application viability. It is shown that it is possible to design a shielding configuration that achieves a high mitigating level with a negligible impact on the motor efficiency and developed torque. Furthermore, comparing calculation models of different complexities, the paper also shows the importance of representing all capacitive couplings inside the motor and the non-uniform current distribution in the shield to determine its effectiveness. Since a large fraction of the motor failures are caused by bearing currents, this paper can provide benefits to key topics for industry, such as equipment reliability and availability.

Index Terms — Electrostatic shield, finite element method, bearing currents, common mode currents, induction motor.

I. INTRODUCTION

Due to the presence of voltage pulses with extremely short rise times (several kV/μs) in motors driven by inverters, harmful effects on the operation and life of electric machines have been identified in the last few decades. The typical problems include (i) transient overvoltages at the motor terminals and their non-linear distribution along the coil [1] and (ii) the high frequency current circulation in the system, which, depending on the related paths, can be classified in different ways and generate distinct problems to the drive system. As an example, if the motor's and/or the load's bearings are part of their paths, such current flow can cause serious problems to these parts, as reported in [2] and [3].

The phenomena of inverter-induced bearing currents have been investigated since the nineties [4]. This problem has been consolidated over the years as a specific area of research, and a very good review on this topic can be found in [5] and [6]. In this context, the most accepted nomenclature classifies these bearing currents as: 1) small capacitive bearing currents; 2) electrostatic discharge machining (EDM) currents; 3) circulating bearing currents and 4) rotor ground currents.

Several solutions have been proposed to minimize the inverter-induced bearing currents, such as the use of common mode voltage filters [7], [8]; insulated bearings [9]; motor shaft grounding [10]; additional impedance insertion for common mode current reduction [11] and electrostatic shielding [12] – [17]. It is this last solution, shielding, on which this paper focuses

In general, the shielding solution consists of inserting a conductive material at the slot opening and/or internal surface to change the parasitic capacitive couplings that are formed inside the motor. Thus, depending on the shield location, two forms for their application can apply. One of them is characterized by inserting the conductive material between the stator winding and the rotor. In this case, the main goal is to reduce the stator winding-to-rotor electrostatic coupling to minimize possible EDM currents, as shown in [12] – [14]. In the second one, the shield is placed inside the slot, between the stator winding and core. As will be discussed in section III, with this arrangement the aim is to minimize the circulating bearing currents. This application has not been covered well in literature. The only work found that dealt with this solution is presented in [17]. It is worth noting that, although the shielding devices are generally attributed to squirrel cage induction motors, similar concepts have also recently been discussed in applications for double-fed induction generators [18] and for permanent magnet motors [19].

Further research is still required for the practical application of such solution. The key points to be addressed are the shielding effectiveness to attenuate the undesired phenomena and its

impact on the motor performance, mainly due to the additional losses resulting from the shield presence.

In general, the studies covering this solution attempt only to evaluate the shielding device effectiveness, as done in [13], [15], and [16], not to address its impact on the motor operation. In fact, only a few papers have combined these two aspects. In the case of [14] and [20], experimental measurements were done to estimate the desired quantities. Only few scenarios could be evaluated, making it difficult to obtain the relationship between the shield parameters and its effectiveness and impact on the motor operation. On the other hand, [17] and [21] employed computational simulations to obtain the desired results, which is more useful in the design stage, since unlimited scenarios can be evaluated for the device improvement, drastically saving development time and costs. However, the modeling adopted in such papers is inadequate, not ensuring accurate conclusions. In [12], the authors of the present paper developed a sophisticated methodology that enables a precise calculation of the shielding effects, but the analysis was restricted to shield types aimed specifically at EDM currents attenuation, and not the circulating currents, which this work addresses.

In this context, the aim of the present paper is to thoroughly evaluate the performance of the shielding to mitigate the circulating bearing currents. The shield effectiveness variation with the frequency and the eddy current losses are calculated for different shield heights, thicknesses, materials, and arrangements. The shield impact on the motor efficiency and torque is also evaluated. All developed models are solved via 2D and 3D Finite Element Analysis, implemented in the COMSOL Multiphysics environment. Good guidelines for the practical design of shielding devices for motor bearing protection against circulating currents are presented herein. Since bearing failures are responsible for almost 50 % of the motor downtime [13], this topic is thus directly related to aspects of reliability and availability, which are key concerns for all industry applications.

II. DESCRIPTION OF CIRCULATING BEARING CURRENTS

Among all stray capacitive couplings formed inside the induction machine, the stator winding-to-frame capacitance (C_{wf}) is predominant [22]. Thus, for each switching event of the common mode voltage (CMV), almost all the common mode current (I_{cmc}) returns by the preferred path formed through the windings - stator core - frame, as shown by I_{wf} in Fig. 1.

For the frequencies at play (up to few MHz), the skin depth becomes extremely small in the stator core. Thus, before reaching the grounded point at the motor frame, the I_{wf} current circulates along a complex path flowing in a zigzag path through the lamination sheet surfaces of the stator core, as illustrated in Fig. 1. When passing through the core laminations, the current I_{wf} excites a circumferential magnetic flux around the rotor. This flux induces a voltage along the shaft (v_{sh}) and, if this voltage is high enough to puncture the lubricating film of the bearing and break its insulating properties, a circulating current (I_{cir}) takes place. This current flows along the loop formed by the stator core - frame - non drive end shield - bearing - shaft - rotor core - shaft - bearing - drive end shield - frame - stator core, as shown in Fig. 1.

Once the circulating currents are generated by induction, they mirror the I_{wf} current, which is the source for the coupling magnetic flux. Therefore, as for I_{wf}, they are in synchronism with the switching events of the common mode voltage. The circulating currents are more likely for larger machines (> 100 kW [23]), in which v_{sh} can easily exceed the bearing threshold voltage level. Depending on the motor size, this current can reach peak amplitudes extending from a few hundreds of mA to a few tens of Amperes [24], with oscillating frequencies up to few MHz [25]. Besides, the current intensities are maximal at low motor speeds, decreasing with rising motor speeds and increasing with rising bearing temperatures [26]. In other words, as the thickness of the lubrication film is reduced, the bearing equivalent impedance is also diminished and, consequently, the circulating current grows. For more information about the circulating current and the other inverter-induced bearing currents, reference [27] should be consulted.

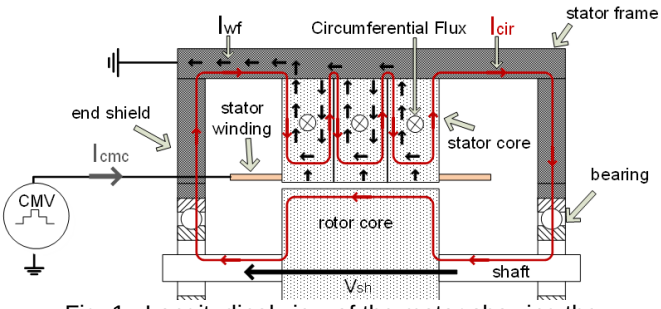

Fig. 1. Longitudinal view of the motor showing the circumferential magnetic flux, induced shaft voltage and circulating bearing current path inside the motor

III. THEORETICAL DESCRIPTION OF THE ELECTROSTATIC SHIELDING FOR CIRCULATING BEARING CURRENTS MITIGATION

The shielding is created by the insertion of a conductive material between the stator winding and core, properly isolated from such parts and grounded at one side. The shield provides a low impedance path for the I_{cmc} current, guiding it directly to the ground, as shown in Fig. 2 by I_{wsh}. By preventing the I_{cmc} current from penetrating the stator core, the magnetic flux around the shaft is minimized. Thus, v_{sh} is attenuated and, consequently, the circulating currents can be suppressed.

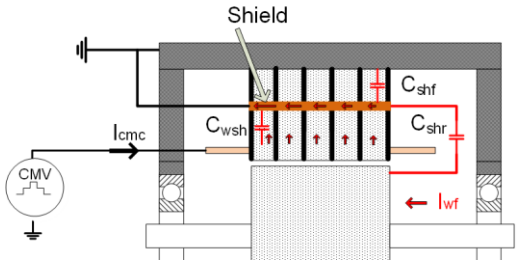

Fig. 2. Shielding actuation to prevent the I_{CMC} current from penetrating the stator core

In addition to the preexisting winding-to-frame, winding-to-rotor (C_{wr}) and rotor-to-frame (C_{rf}) capacitances, as well as the core resistance (R_c) and inductance (L_c), the shield presence introduces new elements inside the motor, forming the electric circuit shown in Fig. 3. These elements are described as the stator winding-to-shield capacitance (C_{wsh}), the shield-to-rotor

capacitance (C_{shr}), the frame-to-shield capacitance (C_{shf}) and the shielding resistance and inductance (R_{sh} and L_{sh}, respectively). The capacitance C_{wf}' represents a residual coupling between the winding and frame in regions not covered by the shield.

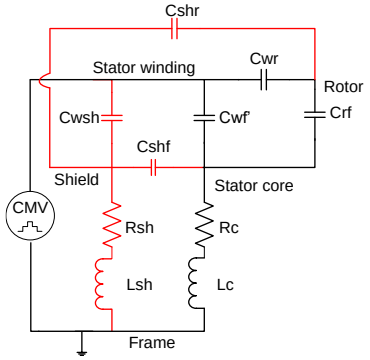

Fig. 3. Proposed equivalent circuit with the additional elements inside the motor due to the shielding device presence

IV. INDUCTION MOTOR AND SHIELDING CHARACTERISTICS

The main parameters of the induction motor used in the simulations are shown in Table I. The stator conductors consist of copper bars and the slot insulation has a relative permittivity of 3. The rotor is a squirrel cage type with semi-closed slot and copper bars. Non-oriented silicon steel M27 is used for the stator and rotor cores.

Two shielding configurations are analyzed. The first is called the “open shield”, and has an inverted “U” geometry, as shown in Fig. 4a. For the second, the shield is completely closed, enveloping all the slot conductors, as illustrated in Fig. 4b. Varying the shield height, thickness and conductive material, performance is evaluated for different situations, shown in the results section.

TABLE I
MAIN PARAMETERS OF INDUCTION MOTOR UNDER STUDY

Rated Power	250 HP	Number of poles	8
Rated Voltage	2.4 kV	Conductors/coil side	6
Rated Current	55.6 A	Coil sides/slot	2
Rated Speed	877 rpm	Insulation Class	F

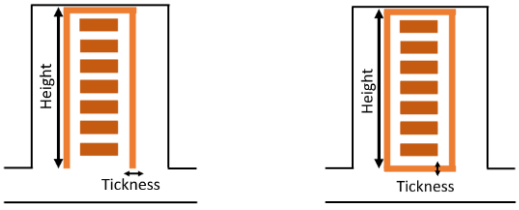

(a) (b)

Fig. 4. Shielding geometry embedded in the stator slot opening. (a) Open shield configuration. (b) Closed shield configuration

V. MOTOR MODELLING FOR THE PROPOSED ANALYSIS

In this section, the developed models to compute the circulating current attenuation and the additional eddy current losses due to the shielding presence are discussed. The 2D and 3D geometries employed in the study, the relevant equations, and the applied boundary conditions, along with other modelling/simulations issues, are described as well.

A. Shielding Effectiveness Calculation - 3D model

The shielding effectiveness (SE) is defined as the ratio of the current amplitude that penetrates the stator core with and without the shielding device presence, as shown by (1).

$$SE = 20\log\left(\frac{I_{c0}}{I_{csh}}\right) \tag{1}$$

where

I_{c0} current (amplitude) that enters the core without the shield presence;

I_{csh} current (amplitude) that enters the core with the shield presence.

To take both the electric and magnetic effects into account, Maxwells equations are solved with an **A**-V formulation in the frequency domain, as shown in (2).

$$\begin{aligned} &\nabla\times\frac{1}{\mu}\nabla\times\boldsymbol{A}+(j\omega\sigma-\omega^2\varepsilon)\boldsymbol{A}+(\sigma+j\omega\varepsilon)\nabla V=\boldsymbol{J_e}\\ &-\nabla.\left((j\omega\sigma-\omega^2\varepsilon)\boldsymbol{A}+(\sigma+j\omega\varepsilon)\nabla V-\boldsymbol{J_e}\right)=0 \end{aligned} \tag{2}$$

where

A magnetic vector potential;

J_e external current density;

V electric potential;

ω source angular frequency;

μ magnetic permeability of the material;

σ electrical conductivity of the material;

ε electrical permittivity of the material.

Since the shield is placed in the stator slot along the active part of the machine, the problem is solved with a single-slot 3D model developed in this work, shown in Fig. 5. For each frequency of interest, the potential $V_{S_1} = 1\ V$ is applied on the coil surfaces and the amplitude of the core current (I_c) is calculated with and without the shield presence. Therefore, the SE can be estimated, which is presented in the results subsections. To represent the shield grounding, the potential $V_{S_2} = 0\ V$ is applied to the S_2 surface. The rotor surface is assumed as being a floating potential. Thus, the potential along S_3 is constant. To represent the core impedance, circuit elements are connected to the S_4 surface, as illustrated in Fig. 5a by R_c and L_c. This impedance is calculated using the formulation presented in [28]. All other surfaces are treated as insulators, including the opposite end of the shield that is not grounded, implying that $\boldsymbol{n}.\boldsymbol{J} = 0$ at these boundaries. Due to the small penetration depth at high

frequencies, it was assumed that the magnetic flux cannot cross the slot boundary. Hence, the condition $\boldsymbol{n} \times \boldsymbol{A} = 0$ is imposed.

B. SE calculation – Equivalent circuit model

Employing the proposed circuit of Fig. 3, the SE is obtained and the results are compared to the values found with the developed 3D model and also with the analytical formulation described in [17].

In the case of the present work, except for the core impedance (R_c and L_c), all circuit parameters are determined using the 3D single slot geometry of Fig. 5. The capacitances are evaluated solving an electrostatic problem in a similar way to that performed in [12]. The shield impedance is determined with the same A-V formulation shown in (2) and discussed above. For each evaluated frequency, the total current flowing through the shield, the heat losses and the magnetic energy generated by this current are computed. In this way, R_{sh} and L_{sh} can be calculated.

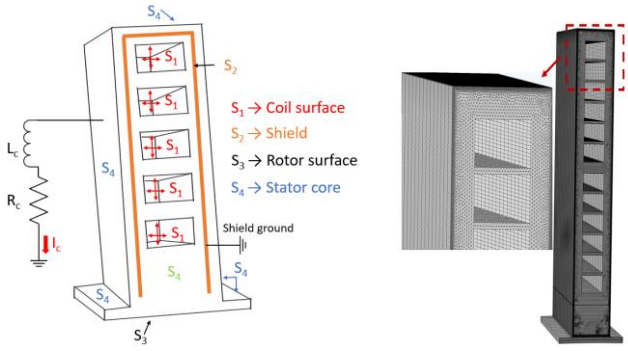

(a) (b)

Fig. 5. Single-slot geometry for the investigation of the shielding effectiveness variation with frequency. (a) Slot surfaces for the applied boundary conditions (b) Finite element mesh used

C. Model for the shield losses calculation

To compute the shield eddy current losses and evaluate its influence on the motor performance, all the magnetic flux that penetrates the slot region must be determined. Thus, in addition to the fundamental-frequency leakage and main air-gap flux, the time and space harmonic fluxes must be included in the calculations. Therefore, to take all these aspects into account, a time-stepping analysis is applied.

Once the shield is inserted into the slot, a 2D approximation modelling the motor cross-section area is satisfactory for the loss calculation. The partial differential equation describing the magnetic vector potential distribution in the region of interest is given by (3).

$$\nabla \times \frac{1}{\mu} \nabla \times \boldsymbol{A} + \sigma \frac{\partial \boldsymbol{A}}{\partial t} - \sigma \frac{u_c}{l_c} = 0 \qquad (3)$$

where

u_c electrical potential difference between the ends of a conductor;

l_c conductor length.

For the analyzed motor, the stator winding is supplied by a voltage source at the nominal value (2.4 kV). In addition, all conductors of the same coil as well as all the coils of the same phase are connected in series. The rotor conductors are interconnected by circuit elements that represent the end ring resistance between two adjacent bars.

To avoid high eddy currents circulation in the shield, the conductive plates are interconnected only at one of their ends. Thus, in the shield region, the induced currents form loops that are restricted to each individual plate. Therefore, the total current in any cross-section of these plates must be zero. To simulate this behavior, a null current source is impressed at every shield domain.

The conductivity of the laminated core is neglected. The reaction field caused by eddy currents in the iron is negligible [29] and, thus, the inclusion of iron losses in the field solution affects only marginally the calculation of the motor current, power factor, copper losses and rotational speed [30].

Due to symmetry, the motor representation can be made considering only one pole. The stator and rotor equations are solved in their own coordinate systems. A boundary condition over the air gap is used to enforce the continuity of the field solutions. The rotor is rotated at each time step by an angle corresponding to the desired mechanical angular frequency, allowing its continuous movement.

It is worth mentioning that, in addition to the conductor losses calculation, the 2-D finite element modelling methodology developed in this work also allows the computation of the motor torque, also allowing the study of the influence of the shielding device on the resultant torque.

VI. SIMULATION RESULTS AND ANALYSIS

The results presentation is divided into three parts. The main differences between the use of the proposed models in contrast to other formulations found in the literature is discussed in section A. In section B, only the models proposed in this paper are employed. A case study is then developed showing the relation between the shield effectiveness and its additional losses for different shield configurations (open and closed), geometrical dimensions and conductive material. Finally, in section C the possible negative impacts of the shield on the motor performance are evaluated. To achieve this goal, the motor efficiency and developed torque are estimated considering the same shield arrangements presented in section B.

A. Considerations on the SE and shield losses calculation

To illustrate the gains that are achieved with the use of the proposed methodology, the results obtained employing the developed 3D FEM model are compared to those found when using the analytical formulation (AF) described in [17]. First, a detailed analysis for the SE calculation is performed; then, some considerations are made on the shield losses estimation.

1) *SE Calculus Comparisons:* Initially, a simulation is performed employing an aluminum open shield configuration of 48 mm high and 0.1 mm thick. As can be seen in Fig. 6, the 3D FEM model ("open - FEM" curve) leads to results very different from those obtained by the analytical formulation ("AF" curve). In the AF, the analyzed circuit is extremely simplified since it considers that the shield can completely suppress the C_{wf}' and C_{wr} couplings (see Fig. 3). However, for the open shield, there is

always a residual coupling between the winding and frame, formed in the regions not covered by the shield. In addition, the open configuration has nearly no influence on C_{wr}.

Next, the same shield arrangement is analyzed, but with a closed configuration. In this case, C_{wf}' and C_{wr} are eliminated, and the 3D FEM model more closely compares to the AF. Observing Fig. 6, although the SE obtained with the 3D FEM model ("closed - FEM" curve) closely matches the AF results, there are still large differences between the corresponding curves. Such difference is due to the methodology premise of the AF to calculate the shield resistance and inductance, where R_{sh} and L_{sh} are obtained considering that the same current is entering the shield on one side and leaving it through the other side. However, since the winding-to-shield capacitance is distributed along their lengths, the current leaving the shield at its grounded terminal is higher than the current entering in its opposite end. Thus, in the AF the shield impedance value is overestimated. With a higher shield impedance, the SE calculated in the AF is lower than the curve obtained by the FEM model, as illustrated in Fig. 6. Therefore, aiming to account for all the described phenomena, the circuit parameters used in the AF were recalculated employing the methodology showed in section V. In this case, the curve "AF – parameters calculated with FEM" (Fig. 6) shows the SE variation with frequency for the same closed shield analyzed before. As can be seen, when using the proposed parameter calculation methodology, the SE curve estimated with the AF circuit is almost the same as that obtained directly using the 3D FEM model.

Finally, employing the same open shield configuration analyzed before, the SE is determined using the equivalent circuit proposed in this work, shown in Fig. 3. The parameters are calculated with the methodology developed in section V and the obtained results are shown in the curve "Proposed circuit" of Fig. 6. Considering all the appropriate capacitive couplings and the correct current distribution in the shield, the results obtained with the proposed circuit are almost the same as those found with the 3D FEM model.

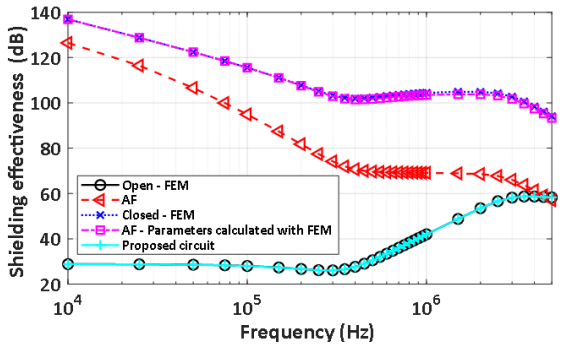

Fig. 6. Shielding effectiveness variation with frequency for different models

2) *Considerations on the shield losses calculation*: By modelling the motor geometry, the rotor movement, the non-sinusoidal sources and the non-linearity of the materials in the time domain analysis, it is possible to reproduce the effects related to the motor time and space harmonics on the losses computation. As stated in [12], the inclusion of such effects leads to dramatic differences in the calculated eddy current losses, in such a way that the use of simplified frequency domain models, as done in [17], is emphatically not recommended, for the sake of accuracy.

To better understand the conclusions described above, Table II shows the shield losses and the amplitude of the fundamental frequency current using three different calculation models. In the first, a frequency domain (FD 60 Hz) model is employed, in a similar way to that performed in [17]. In this case, (i) the core is assumed with an infinite permeability, (ii) only the fundamental-frequency slot leakage flux is considered to produce the shield losses and (iii) the coils are excited by sinusoidal current sources at the fundamental frequency. The second simulation uses the 2D time domain model discussed in section V, which considers the rotor movement and the iron core saturation. In this case, the stator winding is supplied by a sinusoidal voltage source corresponding to the motor rated value. The third simulation repeats the second, but with non-sinusoidal sources. In this case, a PWM voltage is applied with a fundamental component identical to the voltage used in the previous simulation. The PWM switching frequency was defined as 5 kHz and, to ensure a good resolution and simulation accuracy, a time step of 4 μs was set. All simulations use an aluminum open shield configuration of 48 mm high and 0.1 mm thick.

TABLE II
Shielding Losses Results for Different Models

Aluminum open shield – 48 mm high, 0.1 mm thick	FD 60 Hz	TD 60 Hz	TD PWM
Calculated Losses	0.37 kW	0.42 kW	1.53 kW
Stator current (60 Hz)	57.0 A	57.0 A	56.7 A

Although the use of the FD 60 Hz formulation allows a very time efficient model, the assumed simplifications incorrectly estimate the shielding losses, due to two critical problems. First, the FD 60 Hz simulation only accounts for the fundamental-frequency slot leakage flux. In addition, the main air-gap flux which penetrates the slot also produces eddy-current losses in the shielding device, as illustrated in Fig. 7 (in Fig. 7, the flux density distribution is presented as equipotential lines of the magnetic vector potential).

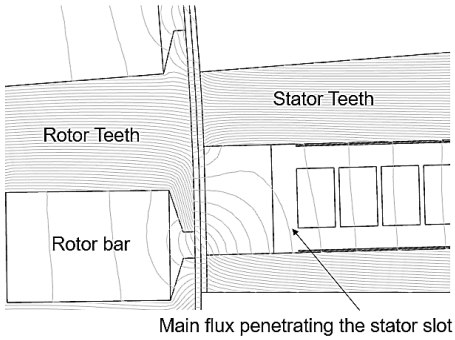

Fig. 7. Flux representation using magnetic equipotential lines

The second problem is related to the fact that the developed FD 60 Hz analysis does not allow for the computation of the shielding losses generated by the high-frequency flux associated with the higher harmonic components. However, by modelling the rotor movement and the actual nonlinear material in the time domain analysis, it is possible to include these effects on the calculations. Thus, the losses obtained employing the time

domain model (TD 60 Hz) were 13 % greater than the estimated value in the first case (FD 60 Hz). Finally, the consideration of a non-sinusoidal source (TD PWM) inserts time harmonic fluxes that led to an increase of 264 % of the obtained losses when compared to the TD 60 Hz model.

Considering the slot region, both the fundamental main flux and space harmonic flux densities are highest near the air gap, as stated in [31]. Since only a small part of the analysed shield is positioned close to the slot opening area, such flux has a minor influence on the shield losses. This explains the small difference between the results obtained with the FD 60 Hz and the TD 60 Hz models, as observed in Table II. On the other hand, the time harmonic fluxes mostly flow circumferentially from one stator tooth to another, as shown in [31]. In this way, the time harmonic fluxes can cross almost all the shield plates that are embedded in the slot. Thus, as shown in Table II, the harmonic fluxes that come from the PWM supply have a significant importance to the shield losses.

B. SE and shield losses calculation for different geometrical dimensions and shielding materials – case study

Considering the discussion presented in the previous section, all simulations for the SE calculation to be shown employ the single-slot 3D FEM model developed in this work. The losses estimation is performed using the time domain model with PWM voltage source. For all cases of losses computation, the motor is considered at rated voltage and speed.

1) *Shield Height Variation Analysis:* First, the analyses are carried out using an aluminum open shield configuration, with 0.1 mm thick and three different heights: 28 mm, 48 mm, and 55 mm. Then, the 48 mm and 55 mm height are also evaluated in the closed configuration.

For the open configurations, as the shield height decreases, there is an increase in the winding-to-frame coupling (C_{wf}') and, therefore, an increase in the current that penetrates the stator core. Thus, in these cases, the SE decreases when lowering the shield height, as shown in Fig. 8. On the other hand, for the closed shield, the winding-to-frame and winding-to-rotor couplings are suppressed (C_{wf}' = C_{wr} = 0). Therefore, unlike what happens for the open arrangement, the shield resistance and inductance have a significant influence on the SE for all analyzed frequencies. Since the shield impedance presents only a slight change for the 48 mm and 55 mm heights, the SE is almost the same for these closed configurations.

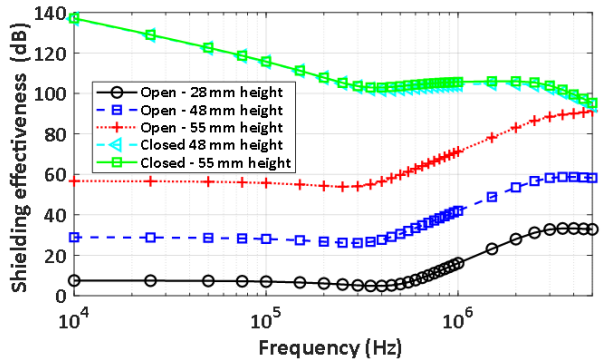

Fig. 8. SE variation with frequency for different shield heights

As observed in Fig. 9, the shield losses increase with the increasing in the height for both open and closed configurations. As the shield height grows, more magnetic flux crosses its surfaces and, thus, greater eddy currents are induced in the shield. To illustrate that, Fig 10 shows the field lines inside one stator slot for the open shield with heights of 28 mm and 55 mm, at the same time instant. The taller shield configuration (55 mm) reaches losses values greater than 200 % in comparison with the height of 48 mm. Also, there is more than a 2000 % increase in the losses from the smallest (28 mm) to the tallest shield (55 mm).

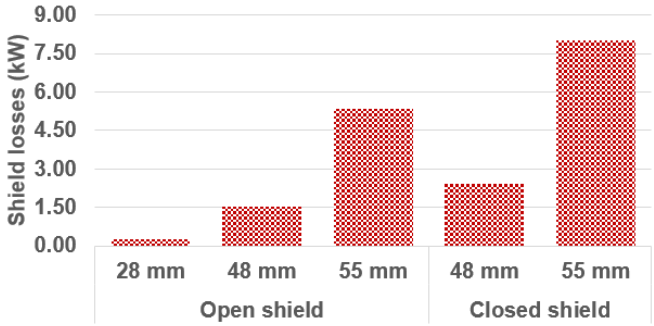

Fig. 9. Shield losses variation for different heights

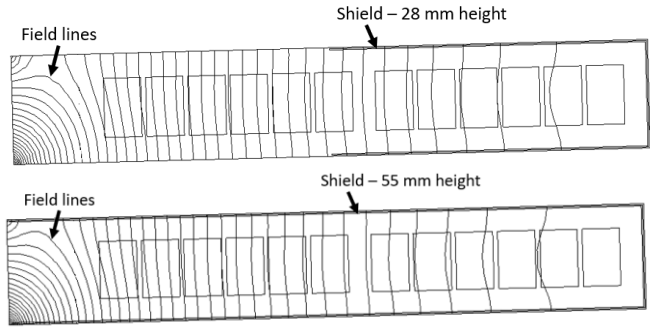

Fig 10. Magnetic field lines inside the slot for two open shield heights

In addition to the flux that passes through the shield from one stator tooth to the other, a radial flux also contributes to the losses, mainly in the slot openings. Also, the effects of both space and time harmonic fluxes, are more intense near the air gap [31]. Therefore, since the additional part of the closed shield configuration is inserted near to the slot openings, it is noted an increase between 50 % and 60 % in the losses compared to the open arrangement.

2) *Shield Thickness Variation Analysis:* Here, the performance of an aluminum open and closed shield configurations, with a height of 55 mm and three thickness values (0.025 mm, 0.1 mm, and 0.4 mm) are analyzed. The results are shown in in Fig. 11.

For the open shields, there is only a slight increase in the SE value with the increase in the shield thickness. In this case, although the shielding impedance changes with its thickness, the R_{sh} and L_{sh} elements are negligible for the SE estimation. Also, the core impedance is independent of the shield geometry. Therefore, the slight changes in the SE curves observed for the

open shield are due only to alterations in the capacitances, caused by the thickness variations.

As before, the closed shield results are very different from those obtained with the open configuration. In this case, due to the C_{wf}' and C_{wr} suppression, the shield impedance has a significant influence on its effectiveness for all analyzed frequencies. Up to 300 kHz, the shielding resistance is the predominant part of its total impedance. Since this resistance is smaller for the thicker shields, the closed arrangement shows a SE rise for increased thicknesses, within this frequency range. On the other hand, as the frequency increases beyond 300 kHz, the inductive reactance becomes the most significant part of the total shield impedance. Also, for the higher frequencies, the shield inductance presents similar values for all analyzed thicknesses, due to the skin effect. Thus, for frequencies above 3 MHz, the shield impedance is approximately the same and the SE becomes independent of the thickness, as shown in Fig. 11.

Fig. 12 shows the shield losses variation for the three thicknesses analyzed. Due to the increase in the volume of conductive material, greater eddy current losses are induced in the shield as the thickness increases. Thus, the use of a 0.4 mm thick shield leads to losses of approximately 130% and 55% greater than those obtained for the 0.025 mm and 0.1 mm thick, respectively. It is noted that, as observed for the SE, the shield losses are less sensitive to variations in the thickness than to the changes in the shield height.

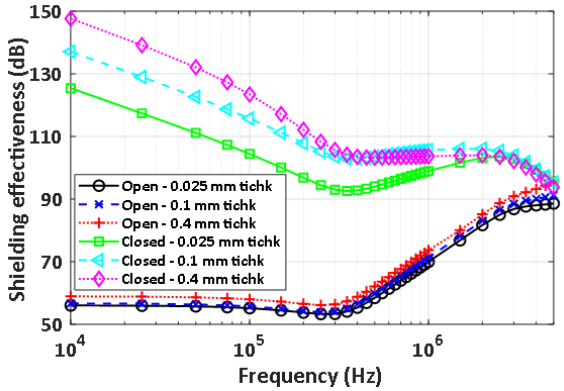

Fig. 11. SE variation with frequency for different shield thicknesses

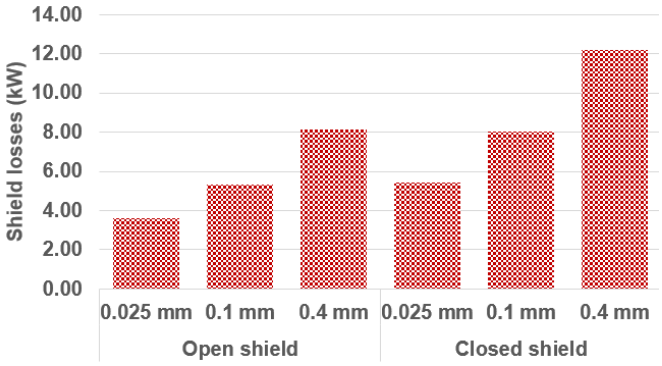

Fig. 12. Shield losses variation for different thickness values

3) *Shield Material Variation Analysis:* Here, the performance of a copper, open and closed shield configurations, of 55 mm height and 0.1 mm thick are analyzed. As shown in Fig. 13, the use of copper is very similar to the results obtained with an aluminum shield. There is only a small increase in the SE of the closed configuration for frequencies up to 300 kHz, due to the lower resistance of the copper shield. In addition, as a consequence of its higher electrical conductivity, the use of copper results in a loss increases of 14 % for the open and 19% for the closed shielding device, as shown in Fig. 14.Since there are no large differences in the SE values calculated with the copper or aluminum shield, the use of the latter is preferable due to the corresponding smaller losses and lower cost.

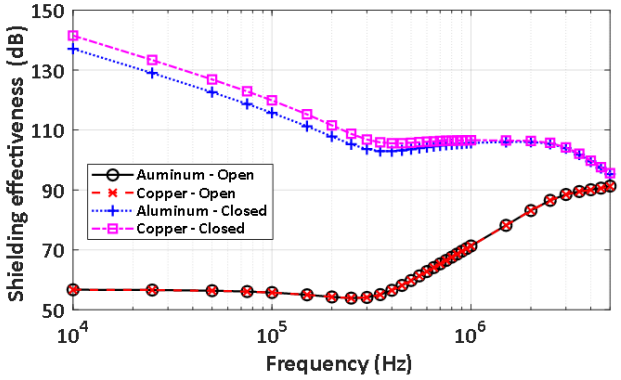

Fig. 13. SE variation with frequency for different shield materials

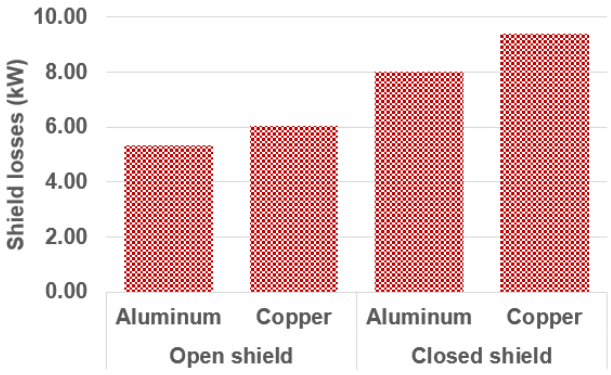

Fig. 14. Shield losses variation for different materials

C. Efficiency and torque impact

Fig. 15 shows the stator winding losses, the rotor bar losses and the total losses for all evaluated cases, including the original configuration (without the shield). Fig. 16 and Fig. 17 present the corresponding reduction of the motor efficiency and torque for all evaluated shield arrangements.

Even though the shields with 55 mm height showed high effectiveness values (always above 50 dB), the additional losses due to the shield presence cause a reduction in the motor efficiency between 1.0% and 4.7% (absolute values), and a decrease from 0.3% to 3.8% (relative values) in the developed torque. On the other hand, for the 28 mm height configurations, the shield has almost no influence on the motor total losses and, consequently, the motor efficiency and torque are kept nearly the same as for the unshielded situation. However, the SE achieved by this configuration may not be satisfactory, especially for the frequencies up to 1 MHz. Therefore, considering the trade-off

relation between the SE and the negative impact on the motor operation, the open shield with 48 mm height appears to be the best solution (for the arrangements simulated). As shown in Fig. 8, for this arrangement (open shield with 48 mm height), the SE remains above 26 dB for all analyzed frequencies. In other words, it ensures an attenuation of at least 20 times the current magnitude that penetrates the stator core. In addition, as shown in Fig. 16 and Fig. 17, this shielding configuration has little impact on the motor efficiency and torque, with a decrease less than 0.1 % in these quantities.

It is important to note that the shielding device has a strong influence on the high-frequency flux components that comes from the PWM supply. As discussed before, such harmonic fluxes flow mostly circumferentially from one stator tooth to another and, consequently, they cross almost all the shield plates. Thus, the induced currents in the shield generate an opposing magnetic field that mitigates these flux components reducing the eddy current losses in the stator winding. Thus, despite the presence of the additional losses added by the shielding device, the decrease of losses in the stator winding, using the open shield with 48 mm height has a negligible impact on the motor efficiency and torque.

VII. CONCLUSIONS

This paper presented a study of the use of electrostatic shields to reduce the high frequency circulating bearing currents of induction machines. From 2D and 3D finite element simulations, several results were obtained, showing the shield effectiveness, the additional losses due to the shield presence and the shield impact on the motor efficiency and torque.

It was shown that for the open shield configuration, the effectiveness significantly decreases with the decrease in its height, but is relatively insensitive to changes in its thickness. In contrast, for the closed shield, the effectiveness does not change with its height and decreases when its thickness decreases. In addition, for both configurations, the use of copper or aluminum hardly changed the effectiveness. For both open and closed configurations, the shielding device losses decreased with the reduction of both shield height and thickness. Even though there are additional losses due to the presence of shielding device, the results show that it is possible to design a shield that ensures a high SE and without negative impact to the motor efficiency and torque.

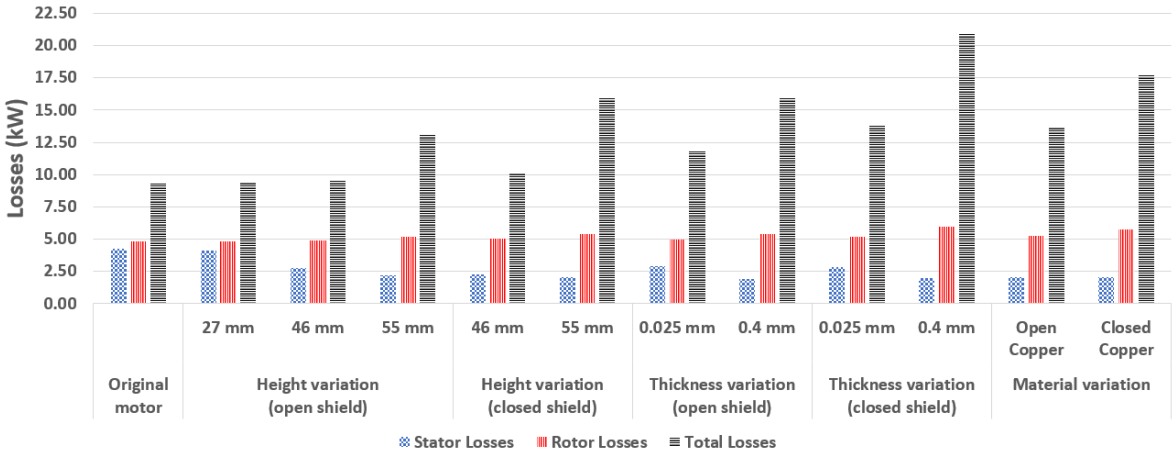

Fig. 15. Stator losses, rotor losses and total losses inside the motor for all analysed cases

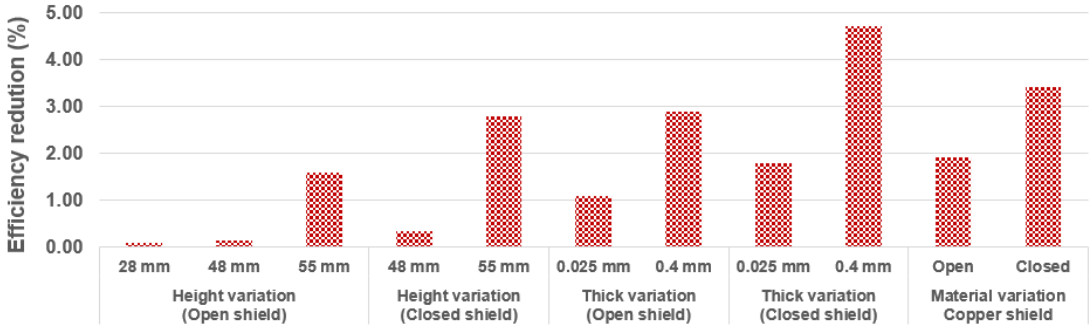

Fig. 16. Motor efficiency reduction due to the shield presence. The reduction figures are presented in absolute percent values.

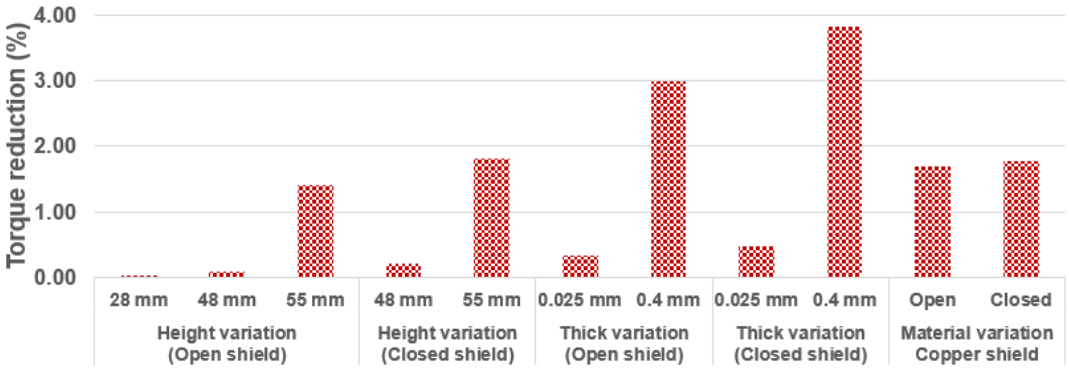

Fig. 17. Motor torque reduction due to the shield presence

VIII. REFERENCES

[1] C. Petrarca, A. Maffucci, V. Tucci e M. Vitelli, "Analysis of the voltage distribution in a motor stator winding subjected to steep-fronted surge voltages by means of a multiconductor lossy transmission line model," *IEEE Transactions on Energy Conversion,* vol. 19, nº 1, pp. 7 - 17, Mar 2004.

[2] R. d. S. Araújo, H. d. Paula, R. d. A. Rodrigues, L. M. R. Baccarini e A. V. Rocha, "Premature Wear and Recurring Bearing Failures in an Inverter-Driven Induction Motor—Part I: Investigation of the Problem," *IEEE Transactions on Industry Applications,* vol. 51, nº 6, pp. 4861 - 4867, Jul 2015.

[3] A. Romanenko, A. Muetze e J. Ahola, "Incipient Bearing Damage Monitoring of 940-h Variable Speed Drive System Operation," *IEEE Transactions on Energy Conversion,* vol. 32, nº 1, pp. 99 - 110, Oct 2016.

[4] S. Chen, T. A. Lipo e D. Fitzgerald, "Source of induction motor bearing currents caused by PWM inverters," *IEEE Transactions on Energy Conversion ,* vol. 11, nº 1, pp. 25 - 32, Mar 1996.

[5] A. Muetze, "Thousands of hits: on inverter-induced bearing currents, related work, and the literature," *Elektrotechnik & Informationstechnik,* vol. 128, nº 11, p. 382–388, Dec 2011.

[6] T. Plazenet, T. Boileau, C. Caironi e B. Nahid-Mobarakeh, "A Comprehensive Study on Shaft Voltages and Bearing Currents in Rotating Machines," *IEEE Transactions on Industry Applications,* vol. 54, nº 4, pp. 3749 - 3759, Mar 2018.

[7] R. d. S. Araújo, R. d. A. Rodrigues, H. d. Paula, B. J. C. Filho, L. M. R. Baccarini e A. V. Rocha, "Premature Wear and Recurring Bearing Failures in an Inverter-Driven Induction Motor—Part II: The Proposed Solution," *IEEE Transactions on Industry Applications,* vol. 51, nº 6, pp. 92 - 100, Jun 2014.

[8] C. Mei, J. Balda e W. Waite, "Cancellation of common-mode Voltages for induction motor drives using active method," *IEEE Transactions on Energy Conversion,* vol. 21, nº 2, pp. 380 - 386, Jun 2006.

[9] J. A. Oliver, G. Guerrero e J. Goldman, "Ceramic Bearings for Electric Motors: Eliminating Damage with New Materials," *IEEE Industry Applications Magazine ,* vol. 23, nº 6, pp. 14 - 20, Nov 2017.

[10] A. Muetze e H. W. Oh, "Design Aspects of Conductive Microfiber Rings for Shaft-Grounding Purposes," *IEEE Transactions on Industry Applications ,* vol. 44, nº 6, pp. 1749 - 1757, Nov 2008.

[11] C. R. Sullivan e A. Muetze, "Simulation Model of Common-Mode Chokes for High-Power Applications," *IEEE Transactions on Industry Applications ,* vol. 46, nº 2, pp. 884 - 891, Feb 2010.

[12] M. T. A. Êvo e H. d. Paula, "Electrostatic shielding for bearings discharge currents attenuation: analysis of its effectiveness, losses and impact on the motor performance – a study for design guidelines," *IET Electric Power Applications, Vol.* 14, no 6, pp. 1050-1059, Jun 2020.

[13] F. J. T. E. Ferreira, M. V. Cistelecan e A. T. d. Almeida, "Evaluation of Slot-Embedded Partial Electrostatic Shield for High-Frequency Bearing Current Mitigation in Inverter-Fed Induction Motors," *IEEE Trans. on Energy Conversion,* vol. 27, nº 2, pp. 382 - 390, Apr 2012.

[14] B. Bai, Y. Wang e X. Wang, "Suppression for Discharging Bearing Current in Variable-Frequency Motors Based on Electromagnetic Shielding Slot Wedge," *IEEE Transactions on Magnetics,* vol. 51, nº 11, Jun 2015.

[15] K. Vostrov, J. Pyrhönen e J. Ahola, "Shielding the end windings to reduce bearing currents," em *International Conference on Electrical Machines (ICEM)*, Gothenburg, Sweden, 2020.

[16] K. Vostrov, J. Pyrhönen, J. Ahola e M. Niemelä, "Non-circulating Bearing Currents Mitigation Approach Based on Machine Stator Design Options," em *XIII International Conference on Electrical Machines (ICEM)*, 2018.

[17] P. Mäki-Ontto e J. Luomi, "Bearing current prevention of converter-fed AC machines with a conductive shielding in stator slots," *IEEE International Electric Machines and Drives Conference, 2003. IEMDC'03,* vol. 1, pp. 274 - 278, Jun 2003.

[18] R. Liu, E. Yang, J. Chen e S. Niu, "Novel Bearing Current Suppression Approach in Doubly-Fed Induction Generators," *IEEE Access ,* vol. 7, pp. 171525 - 171532, Nov 2019.

[19] J.-K. Park, W. Thusitha, S.-J. Choi e J. Hur, "Shaft-to-

frame voltage suppressing approach by applying eletromagnetic shield in IPMSM," em *IEEE International Electric Machines and Drives Conference (IEMDC)*, Miami, FL, USA, 2017.

[20] D. F. Busse, J. M. Erdman, R. J. Kerkman, D. W. Schlegel e G. L. Skibinski, "An evaluation of the electrostatic shielded induction motor: a solution for rotor shaft voltage buildup and bearing current," *IEEE Transactions on Industry Applications,* vol. 33, nº 6, pp. 1563 - 1570, Nov 1997.

[21] B. Heidler, K. Brune e M. Doppelbauer, "Design aspects of an electrostatic shield in an electric machine for hybrid electric vehicles," em *8th IET International Conference on Power Electronics, Machines and Drives (PEMD 2016)*, Glasgow, UK, 2016.

[22] M. Schuster e A. Binder, "Comparison of different inverter-fed AC motor types regarding common-mode bearing currents," em *IEEE Energy Conversion Congress and Exposition (ECCE)*, Montreal, QC, Canada, 2015.

[23] A. Binder e A. Muetze, "Scaling Effects of Inverter-Induced Bearing Currents in AC Machines," *IEEE Transactions on Industry Applications,* vol. 44, nº 3, pp. 769 - 776, May 2008.

[24] A. Muetze e A. Binder, "Calculation of Circulating Bearing Currents in Machines of Inverter-Based Drive Systems," *IEEE Transactions on Industrial Electronics,* vol. 5, nº 2, pp. 932 - 938, Apr 2007.

[25] A. Muetze, V. Niskanen e J. Ahola, "On Radio-Frequency-Based Detection of High-Frequency Circulating Bearing Current Flow," *IEEE Trans. on Ind. Applications,* vol. 50, nº 4, pp. 2592 - 2601, Jul 2014.

[26] A. Muetze e A. Binder, "Don't lose your bearings," *IEEE Industry Applications Magazine ,* vol. 12, nº 4, pp. 22 - 31, Jul 2006.

[27] M. T. A. Êvo, A. M. Alzamora, I. O. Zaparoli e H. d. Paula, "Inverter-induced bearing currents – A thorough study of the cause-and-effect chains," em *IEEE Industry Applications Society Annual Meeting (IAS)*, Vancouver, BC, Canada, 2021.

[28] P. Mäki-Ontto e J. Luomi, "Induction Motor Model for the Analysis of Capacitive and Induced Shaft Voltages," em *IEEE International Conference on Electric Machines and Drives*, San Antonio, USA, 2005.

[29] K. Yamazaki, A. Suzuki, M. Ohto e T. Takakura, "Circuit Parameters Determination Involving Stray Load Loss and Harmonic Torques for High-Speed Induction Motors Fed by Inverters," *IEEE Transactions on Energy Conversion ,* vol. 28, nº 1, pp. 154 - 163, Mar 2013.

[30] E. Dlala, A. Belahcen e A. Arkkio, "On the Importance of Incorporating Iron Losses in the Magnetic Field Solution of Electrical Machines," *IEEE Transactions on Magnetics,* vol. 46, nº 8, pp. 3101 - 3104, Jul 2010.

[31] M. Islam e A. Arkkio, "Effects of pulse-width-modulated supply voltage on eddy currents in the form-wound stator winding of a cage induction motor," *IET Electric Power Applications,* vol. 3, nº 1, pp. 50 - 58, Jan 2009.

IX. VITAE

Marco Tulio Alves Êvo was born in Patos de Minas, Brazil, on November 13, 1987. He received the B.Sc., M.Sc., and Ph.D degrees in electrical engineering from the e Federal University of Minas Gerais, Belo Horizonte, MG, Brazil in 2011, 2014, and 2020, respectively. He is currently a professor of electrical engineering with the e Federal University of São João del Rei del Rei, MG, Brazil. He has been teaching courses on electrical machines since 2014. His main interests include motor drives, and electromagnetic compatibility.

Caio Eduardo Silva received the B.Sc. degree in Electrical Engineering from Federal University of São João del-Rei (UFSJ), in 2012, and the M.Sc. degree in Electrical Engineering on the Graduate Program in Electrical Engineering of UFSJ / CEFETMG, from UFSJ, in 2015. Since 2014, he has held the position of Electrical Engineer in the Projects and Works Division of UFSJ. Currently is a Ph.D. student the Graduate Program in Electrical Engineering of the Federal University of Uberlândia (UFU). His research interests focus on Motor Drives, Multilevel Inverters, Reliability based on Physics of Failure (PoF), Direct Current Transmission and Electric Drives.

Isabela O Zaparoli was born in Passos, Brazil, in 1993. She received the degree in Electrical Engineering and Master's degree from Federal University of São João del-Rei (UFSJ), São João del Rei, Brazil, in 2016 and 2018, respectively. Currently, she is a scholarship of doctor's degree from Federal University of Uberlândia (UFU). Her main area of research includes online condition monitoring, diagnostics of rotating electric machines and signal processing.

Hélder de Paula was born in Uberlândia, Brazil, on December'75. He received the B.Sc., M.Sc. and Ph.D. degrees in Electrical Engineering from the Federal University of Uberlândia (UFU) in 1998, 2001, and 2005, respectively. From July'06 until November'17 he was with the Electrical Engineering Department of the Federal University of Minas Gerais (UFMG); since then he is a member of the Faculty of Electrical Engineering of UFU. Since April'21 he's been the Vice Chair of the Mining Committee of the Industry Applications Society of the IEEE. His main interests are motor drives, power quality, reliability and underground power transmission.